Theoretical and Applied Fracture Mechanics 75 (2015) 124–136

Contents lists available at ScienceDirect

Theoretical and Applied Fracture Mechanics

journal homepage: www.elsevier.com/locate/tafmec

The effects of thermal stresses on the elliptical surface cracks in PWR reactor pressure vessel

Usman Tariq Murtaza *, M. Javed Hyder

Department of Mechanical Engineering, Pakistan Institute of Engineering and Applied Sciences, Islamabad 45650, Pakistan

ARTICLE INFO

Article history:
Available online 9 December 2014

Keywords:
Corner crack
Thermal stress
RPV

ABSTRACT

In this study, the effects of thermal stresses on the stress intensity factors (SIFs) of the elliptical corner surface cracks postulated at the nozzle-cylinder intersection of a reactor pressure vessel (RPV) were investigated. A typical RPV of a Westinghouse pressurized water reactor and its set-in nozzle were considered for the analysis. The selected set-in nozzle-cylinder intersection for fracture mechanics analysis is also the highest stress concentration point of the RPV. The numerically computed SIFs for a wide range of corner cracks under pressure and combined (pressure plus thermal) loadings are provided as a reference tool for the fracture mechanics design of the RPV. It was also demonstrated that the operational thermal stresses caused by the provision of the annular chamber for the external reactor vessel cooling, actually reduce the SIF of the corner cracks and they do not endanger the safety of the RPV in normal operating conditions.

1. Introduction

It is widely accepted that material flaws, pre-cracks and fatigue cracks initiated at stress concentration points normally lead to catastrophic failure of engineering structures. The semi/quarter elliptical shape is the general representation for surface cracks in engineering structures. Surface cracks in infinite geometries can be analyzed using analytical approaches whereas in finite geometries numerical or experimental techniques [1–3] are inevitably required for the analysis of surface cracks. Similarly, on stress concentration areas, analytical techniques have not been able to provide stress intensity factors (SIFs) for surface cracks because of variable stress fields and higher stress gradients at the crack area. In practical applications there are many components such as reactor pressure vessels (RPV), which are subjected to thermal loadings in addition to mechanical loadings. The fracture analysis of such components is much more involved due to different behavior of cracks under thermal and mechanical loadings [4]. Under such complex loading conditions, a comprehensive and accurate three dimensional finite element analysis (FEA) is required for evaluation of SIFs along the whole crack front.

Inspired by the work of Irwin [5], many researchers have performed the analysis of surface cracks in different geometries and loading conditions during the last five decades. Some of the early studies used techniques such as alternating method [6–8], boundary elements [9–11], virtual crack extension method [12–14], the line spring model [15–17] and the weight function approach [18]. After the availability of finite element methods (FEM) and computers, relatively higher attention has been given to the analysis of surface cracks using FEM [19–23]. In this context, Newman and Raju [24] beautifully fit the extensive data with double series polynomial to produce an empirical equation for the surface cracks. The analysis of surface cracks in pressure vessels is relatively more important as their catastrophic failure essentially leads to the loss of life and property. Many researchers have provided useful SIF solutions for surface cracks in simple cylindrical pressure vessels [25–29].

The researchers [30–34] have also performed structural integrity analysis of RPVs under different normal and accidental conditions such as pressurized thermal shocks. Thermal stresses caused by the injection of emergency cooling water have been considered for the RPV integrity analysis while most of the studies have ignored thermal stresses caused by the normal operating conditions of the plant. The structural integrity of RPV is such a large-scale research project that it is not adequate to fulfill the fracture evaluation in accordance with ASME code [35] and an additional research work should be taken into account for safe operation of the plant.

To investigate the effects of thermal stresses, under normal operating conditions of the plant, on the corner surface cracks at

* Corresponding author. Tel.: +92 51 2207380/4x3414.
E-mail addresses: maniiut@yahoo.com (U.T. Murtaza), hyder@pieas.edu.pk (M. Javed Hyder).

http://dx.doi.org/10.1016/j.tafmec.2014.12.001
0167-8442/

Nomenclature

PWR	pressurized water reactor
ERVC	external reactor vessel cooling
RPV	reactor pressure vessel
RVI	reactor vessel insulation
HSCP	highest stress concentration point
SESC-FP	semi-elliptical surface crack in finite plate
SESC-TP	semi-elliptical surface crack in thick pipe
SIF	stress intensity factor
a	depth of semi-elliptical surface crack/minor axis of the crack
c	half-length of semi-elliptical surface crack/major axis of the crack
t	thickness of the reactor pressure vessel wall at the set-in nozzle intersection
Q	flaw shape parameter
E	Young modulus of the material
L	length of the SESC-TP specimen
R_i	inner radius of SESC-TP specimen
P_{int}	internal pressure
T_{in}	temperature of the inner surface of the RPV
T_{out}	temperature of the outer surface of the RPV
S_b	remote bending stress on outer fiber
S_t	remote uniform-tension stress
K_I	SIF in mode-I
K_I^p	SIF in mode-I under only pressure loadings
K_I^{ps}	SIF in mode-I under combined pressure plus thermal loadings
K_{Ic}	fracture toughness of the material
ϕ	crack face angle, degrees
v	Poisson's ratio of the material

the set-in nozzle-cylinder intersection, a typical RPV [36] of the Westinghouse pressurized water reactor (PWR) is selected for the fracture mechanics analysis. The RPV shown in Fig. 1(a) and (b) is a double loop cylindrical pressure vessel with hemispherical bottom and upper head. The reactor coolant, i.e. pressurized light water, enters the reactor vessel through the set-in nozzle (see Fig. 1) and flows through the reactor core where it absorbs heat. The inlet nozzles usually used in RPVs of PWRs are set-in nozzles (see Fig. 2), which have flange set into the vessel wall [36]. After receiving heat, the reactor coolant leaves the RPV through the set-out nozzle. To prevent the reactor coolant heat from being transferred to the surrounding structures a thermal insulation called reactor vessel insulation (RVI) encloses the RPV. Initially in conventional PWRs, there was no liquid flow path between the RPV and RVI as shown in Fig. 3(a). The concept of external reactor vessel cooling (ERVC) depicted in Fig. 3(a) has been of great interest to nuclear system designers since it provides an efficient solution of accident management issues that have been evolved after the Three Mile Island unit 2 incident [37]. The design concepts of retaining the corium (molten core) inside the RPV, during core melting accident, through external cooling of RPV is called ERVC. Core melting accident is one of the severe accidents in PWRs [38,39]. The space between the RPV and the RVI forms an annular chamber (see Fig. 3(a)) which can be flooded with cooling water in accidental conditions through passive valving which directly cool the reactor vessel in the event of core melting.

In normal operating conditions (non-accidental conditions), the space between the RPV and the RVI is filled with air forming an annular chamber of the air (see Fig. 3(b)). Under normal plant operating conditions the reactor cavity cooling system (VRC) is

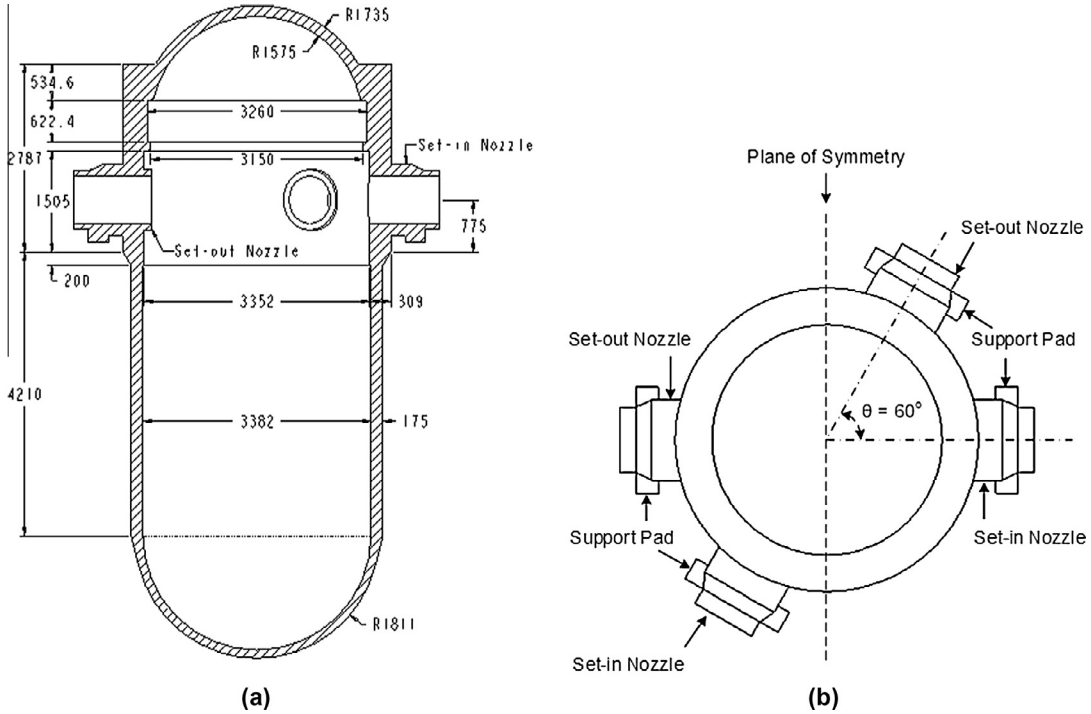

Fig. 1. Engineering drawing of the RPV (a) cut-section view, all dimensions in mm, (b) top view.

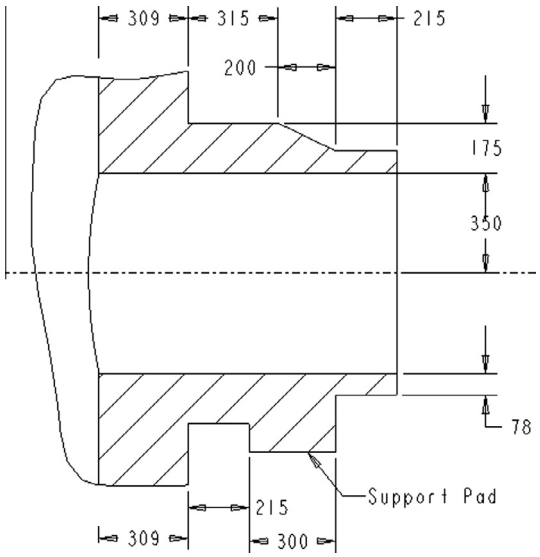

Fig. 2. Engineering drawing of the set-in nozzle, all dimensions in mm.

designed to cool down the RVI. The VRC is a safety related system which reduces the temperature of the RVI lower than or equal to 25 °C. The provision of the annular chamber of air between the hot reactor vessel wall and the cold vessel insulation generates thermal stresses in the RPV wall under normal operating conditions. Since the suggestions of annular chamber for ERVC, the effects of thermal stresses on the structural integrity of the RPV has become an important research area.

In this study, linear elastic fracture mechanics analysis is performed to compute SIFs of the elliptical corner surface cracks postulated at the set-in nozzle-cylinder intersection of the RPV of the PWR. The selected set-in nozzle-cylinder intersection for fracture mechanics analysis is also the highest stress concentration point (HSCP) of the RPV. The numerically computed SIFs for the wide range of corner surface cracks under the only pressure and the combined (pressure plus thermal) loadings are provided under normal operating conditions of the plant. The SIF solutions are presented in a suitable format thus providing a useful tool for fracture mechanics design of the RPV. To the authors' best knowledge, the provided SIF solutions are not available, neither analytically, nor numerically in the contemporary literature.

2. Problem description

The analysis of the RPV has been carried out initially under the only pressure loadings. Subsequently, in order to investigate the effects of operational thermal stresses caused by the provision of the annular chamber for ERVC, the analysis under combined pressure plus thermal loadings (called hereinafter 'the combined loadings') has also been performed.

In order to perform the structural integrity analysis of the RPV, the stability verification at the HSCP of the RPV is mandatory. In order to locate HSCP, initially a stress analysis of the un-cracked RPV has been carried out using ANSYS workbench. The set-in nozzle-cylinder intersection has been found as the HSCP of the RPV. The hoop stress distributions in the RPV under the only pressure and the combined loadings are given in Section 3 that follows.

The fracture mechanics analysis of the RPV has been conducted by postulating forty-eight corner cracks at the HSCP including the worst case crack allowed by the Appendix G ASME III, Div. 1 [40]. The magnitude and distribution of the SIFs along the whole crack fronts for all the forty-eight cracks under the only pressure and the combined loadings were computed numerically using ANSYS workbench.

2.1. Material model and boundary conditions

The material selected for the RPV of the PWR is SA-533 Gr.B Cl.1, a nuclear grade steel having nominal composition (Mn – ½

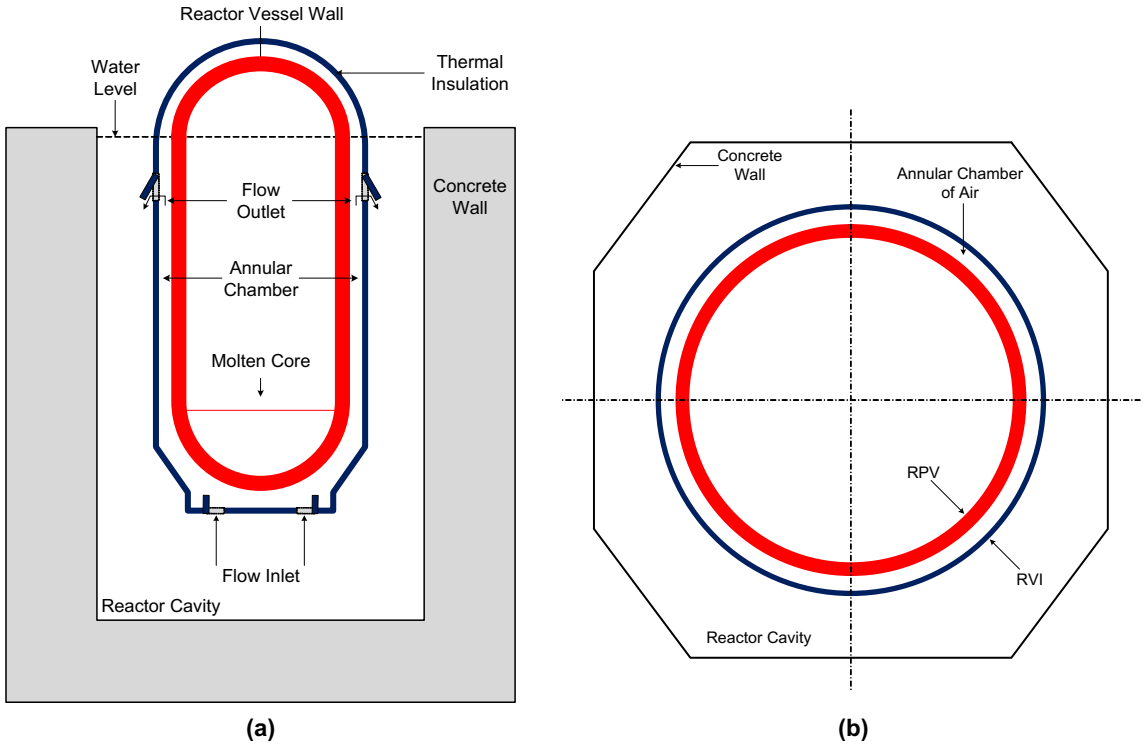

Fig. 3. Schematic diagram (a) water flow path under ERVC, (b) annular chamber of air under normal operating conditions.

Table 1
Mechanical and thermal properties for SA-533B Cl.1.

Temperature (°C)	Young's modulus (GPa)	Poisson's ratio	Conductivity (W $(m \times °C)^{-1}$)	Ins. Coefficient of thermal expansion (1/°C)
300	183	0.3	38.7	15.1×10^{-6}
250	187	0.3	39.5	14.8×10^{-6}

Mo – ½ Ni). The linear elastic material model was used for the stress analysis and for the fracture mechanics analysis of the RPV. The mechanical and the thermal properties of the selected material [41] are given in Table 1.

The following boundary conditions (B.Cs) have been applied for the numerical computations in this study:

1. Taking the advantage of the geometric and loadings symmetry, as shown in Fig. 1(b), only half of RPV is modelled for FEA.
2. The internal pressure taken for the analysis is equal to P_{int} = 17.16 MPa which is equal to the design pressure of the RPV.
3. The movement of the vessel support pads (see Fig. 1(b)) are fixed in all direction.
4. The temperature of the RPV is taken equal to 288 °C. Initially, applying no temperature difference between the inner and outer surface of the RPV, SIFs (K_I^p) based on only pressure loadings have been computed and are provided in Section 4.3.
5. To investigate the effect of thermal stresses in the RPV wall, under normal operating conditions, the temperature of the inner surface of the RPV was taken as T_{in} = 288 °C while the temperature of the outer surface of RPV was taken as T_{out} = 276.5 °C. The applied temperature difference ΔT = 11.5 °C is normally encountered in the RPV wall under normal operating conditions provided that the air clearance between the RPV and the RVI (see Fig. 3(b)) is t_{air} = 150 mm [38]. The SIFs under the combined (pressure plus thermal) loadings have also been computed and are provided in Section 4.4.

3. The stress analysis of the un-cracked RPV

3.1. Stress analysis under the only pressure loadings

Stress analysis of the RPV under only pressure loadings has been performed in this section. To achieve an overall brick/hex mesh for FEA, the complex RPV geometry is decomposed into several sweepable bodies. The full 3D Finite Element (FE) hex mesh model of the RPV having skewness equal to 0.801 is shown in Fig. 4. The value of the skewness ranges from 0 to 1, the smaller the better, and the FE model having skewness less than 0.95 are acceptable for FEA [42]. As the FE model of the RPV has skewness less than 0.95, hence it is an acceptable model for FEA. The FE model of RPV contains a total of 37,557 finite elements and 186,332 nodes. The element type used for the stress analysis is Solid-186 which is a higher order 3-D, 20 node solid element with midside nodes and curved edges. The hoop stress distributions in the RPV under only pressure loadings are shown in Fig. 5.

3.2. Stress analysis under the only thermal loadings

Stress analysis of the RPV under only thermal loadings has been performed, in this section, using the same FE model as shown in Fig. 4. The temperature distributions in the nozzle belt of the RPV resulted from the FEA are shown Fig. 6(a). These temperature distributions are used for calculating the thermal stress in the RPV. The thermal stress distributions in the hoop direction in the nozzle belt of RPV are shown in Fig. 6(b).

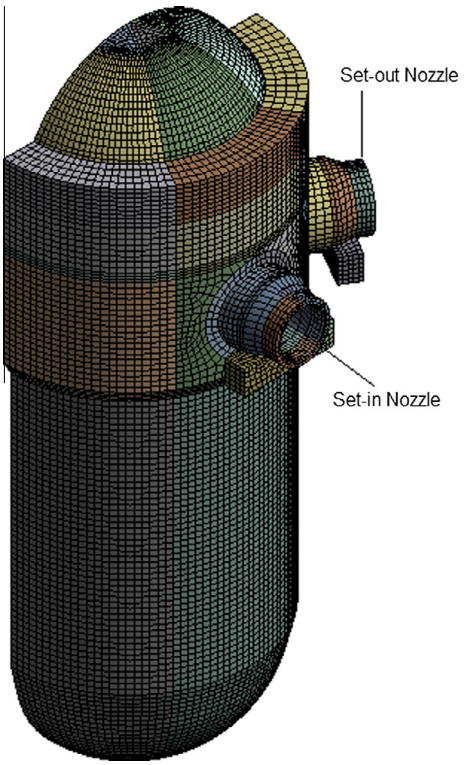

Fig. 4. 3D solid-186 finite elements model of the RPV.

3.3. Stress analysis under the combined loadings

In this section, the stresses that are produced in the RPV under the combined loadings have been determined. The structural pressure stresses have been coupled with the thermal stresses and the resulting hoop stress distributions under the combined loadings are shown in Fig. 7.

It is evident from Figs. 5–7 that the set-in nozzle-cylinder intersection is the HSCP of the RPV under the only pressure as well as the combined loadings.

4. Numerical calculation of the SIFs

4.1. Modelling approach

The development of the fracture model used in this study contains six steps (see Fig. 8) which are briefly described below:

Step No. 1: Modelling of the un-cracked engineering structure.
Step No. 2: Modelling of the crack profile body according to the crack's dimensions. The crack faces are needed to be coincident at the crack front. The width of the crack body is taken "1 mm".
Step No. 3: For modelling of surface crack in the structure, crack profile body (generated in step 2) should be subtracted from the un-cracked structure.
Step No. 4: For modelling the pallet bodies around the crack front as shown in Fig. 8(d), a tube-like volume (hereinafter called 'the tube') is swept around the crack front initially. The

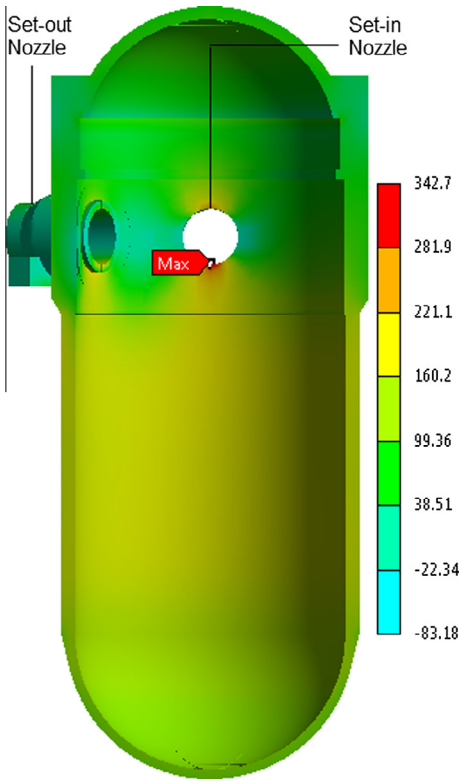

Fig. 5. Hoop stress distributions under the only pressure loadings, stresses in MPa.

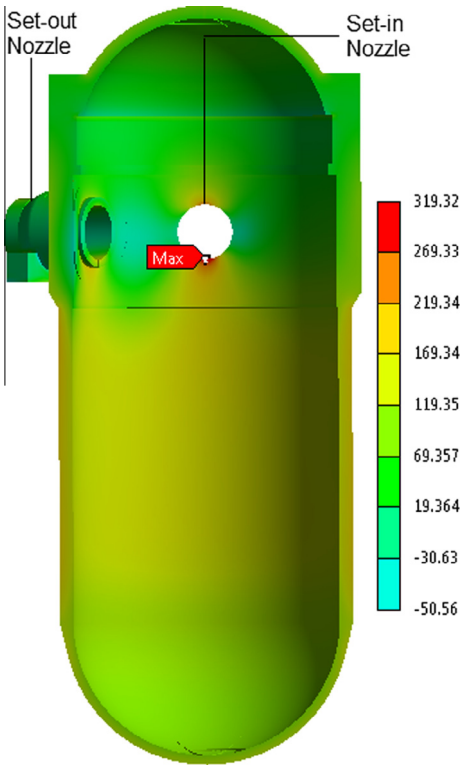

Fig. 7. Hoop stress distributions under the combined (pressure plus thermal) loadings.

radius of the tube is dependent on the curvature of the crack front. A limiting radius exists for the tube around an elliptical crack front. The tube radius is not fixed and changes as the "*a*/*c*" ratio (see Fig. 9) of the elliptical crack changes. The skewness of the FE mesh around the crack front is dependent on the radius of the tube. The radius of the tube which leads to a mesh of skewness equals to 0.50 is taken for the fracture model in this study. After the successful modelling of the tube around the crack front, it is further sliced into small pallet shape bodies (hereinafter called 'the pallets'). The pallets are generated in such a way that the ends of the pallets should be perpendicular to the crack front. The local coordinate system of the pallets is shown in Fig. 8(d). The divisions of the crack front and hence the number of pallets may vary in the range of zero to infinity. Increasing the number of pallets will decrease the skewness value and hence will improve the mesh quality. One hundred and twenty pallets are generated along the semi-elliptical surface crack in this study as shown in Fig. 8(d).

Step No. 5: The sweepable pallets (generated in step no. 4) are filled with sweep mesh using purely quadratic hexahedral/brick Solid-186 (20 node) elements. The brick elements are ordered in layers around the crack front. The skewness of the FE mesh is also dependent upon the number of layers. In this fracture model, six layers of equal height are generated in each pallet body as shown in Fig. 8(e). The first layer, around the crack front, is meshed using hexahedral wedge-shaped (20-node collapsed quarter point) singular elements which exhibit $1/\sqrt{r}$ behavior where r is distance from the crack front as shown in

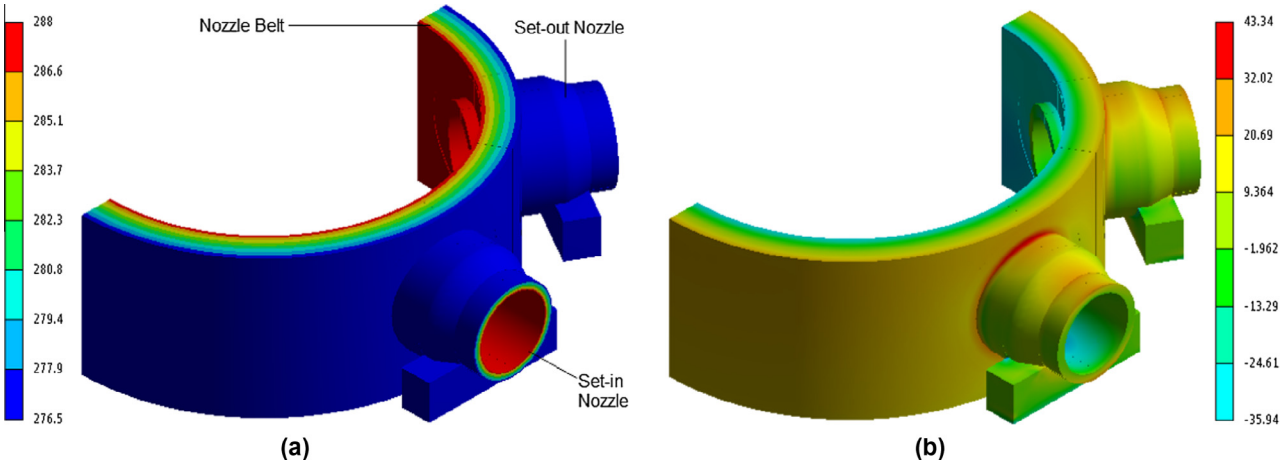

Fig. 6. (a) Temperature distributions in nozzle belt, temperature in °C, (b) thermal stress distributions in hoop direction, stresses in MPa.

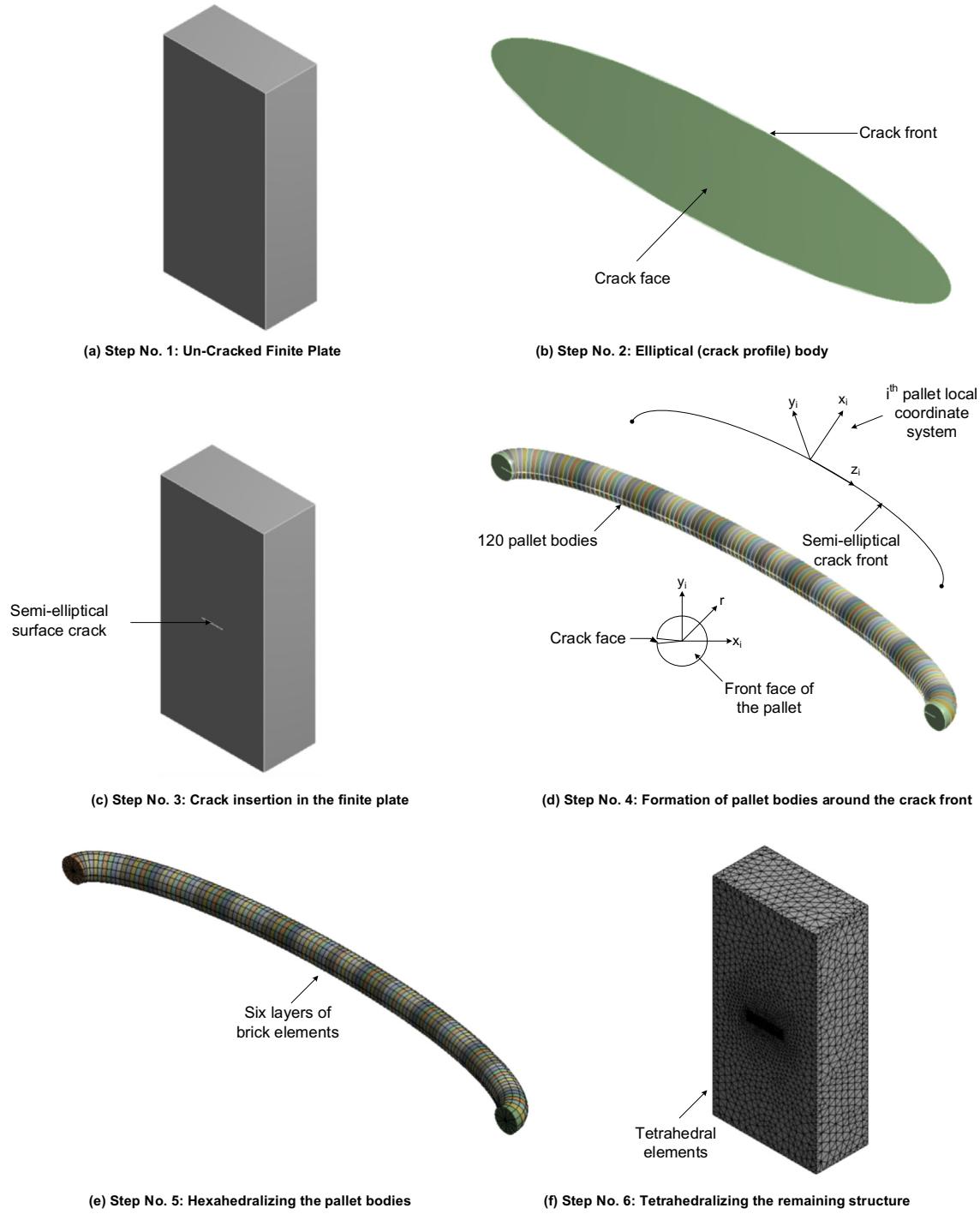

(a) Step No. 1: Un-Cracked Finite Plate

(b) Step No. 2: Elliptical (crack profile) body

(c) Step No. 3: Crack insertion in the finite plate

(d) Step No. 4: Formation of pallet bodies around the crack front

(e) Step No. 5: Hexahedralizing the pallet bodies

(f) Step No. 6: Tetrahedralizing the remaining structure

Fig. 8. Steps to develop the fracture model.

Fig. 8(d). Such elements are essentially required as stress and deformation fields around the crack front generally have high gradients. The stresses and strains are singular at the crack front varying as $1/\sqrt{r}$. To capture this singularity in stresses and strains, singular elements around the crack front are inevitably required.

Step No. 6: The volume around the multi-body refine tube, is meshed using quadratic tetrahedral Solid-187 (10 node) elements.

Once the layers of higher order brick elements are generated around the crack front, these layers are used as volumes for *J*-integral evaluation. The *J*-Integral evaluation is based on the domain integral method by Shih et al. [43]. The domain integration formulation applies volume integration for 3-D problems to calculate *J*-Integral value. Finally SIFs (K) along the whole crack front are evaluated by Eq. (1).

$$K = \sqrt{\frac{J \cdot E}{(1-\nu^2)}} \tag{1}$$

where J = Value of *J*-integral around the crack front [44].

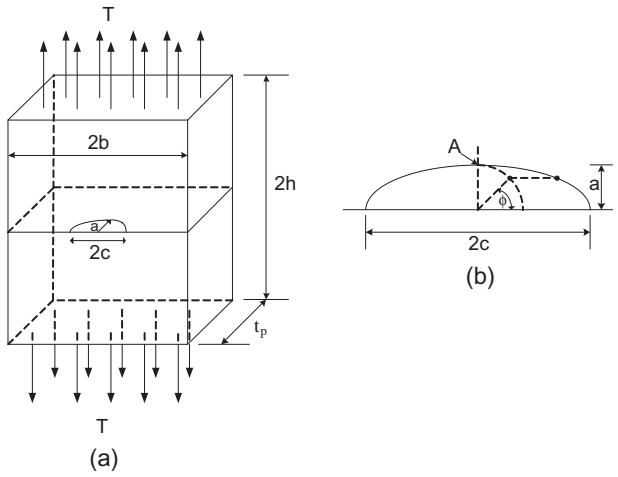

Fig. 9. (a) SESC-FP specimen, (b) crack tip position parameters in SESC-FP specimen.

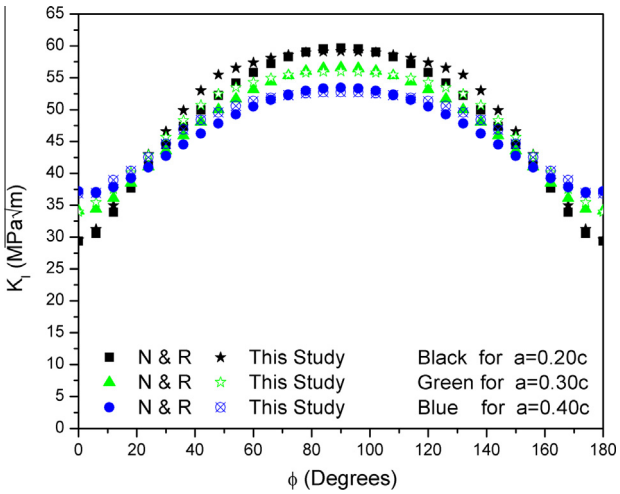

Fig. 11. Comparison of the developed fracture model with Newman and Raju analysis.

4.2. Verification of the fracture model

In order to validate developed fracture model, the following two problems are solved initially;

(1) Semi-elliptical surface crack in finite plate.
(2) Semi-elliptical surface crack in thick pipe.

The SIF solutions of aforesaid two problems are available in the literature. For validation purpose, the results are compared with the available well-known solutions and are presented in the following Sections.

4.2.1. Semi-elliptical surface crack in finite plate

Different solutions exist in the literature for computation of SIF of a semi-elliptical surface crack in a finite thickness plate under uniform tension as shown in Fig. 9. Among them, an empirical equation proposed by Newman and Raju [45] is available and is still most widely used for comparison and validation purposes. The empirical relationship presented in Ref. [45] is reproduced here for reference;

$$K_I = (S_t + HS_b)\sqrt{\pi \frac{a}{Q} F\left(\frac{a}{t_p}, \frac{a}{c}, \frac{c}{b}, \phi\right)} \tag{2}$$

where Q is given by $Q \cong 1 + 4.593(a/c)^{1.65}$. H and F are as provided by Newman and Raju in Ref. [45]. The semi elliptical surface crack in finite plate (SESC-FP) specimen given in Fig. 9(a), has the dimensions $2b$ = 1000 mm, $2h$ = 2000 mm, t_p = 500 mm, a/t_p = 0.05, T = 100 M.N. The parameters a, c, b, t_p, h, T and ϕ are as given in Fig. 9(a) and (b).

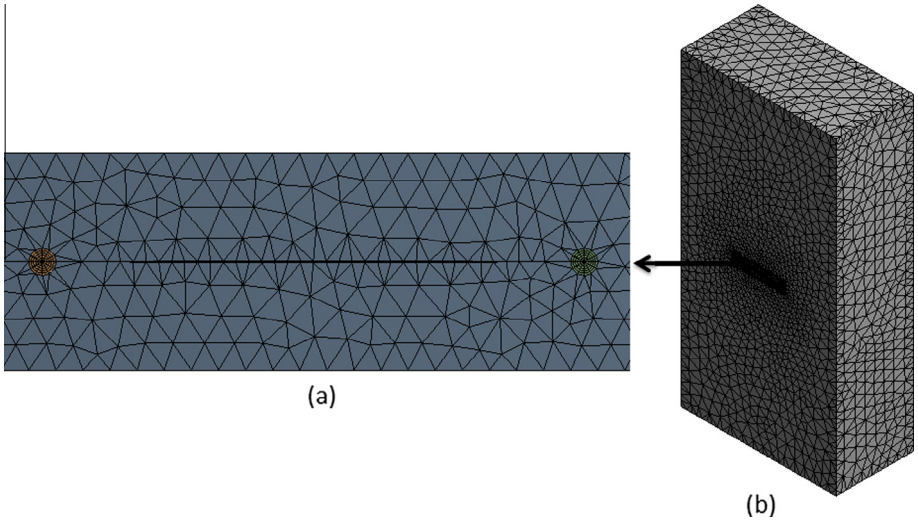

Fig. 10. FE mesh of SESC-FP specimen, (a) close-up view, (b) global view.

Table 2
Details of FE mesh of SESC-FP specimen.

Region	Element type	No. of elements	No. of nodes	No. of layers	No. of pallets
Tube like volume around the crack front	Solid-186	8640	37,189	06	120
Full model including tube like volume	Solid-186 and Solid-187	32,249	70,690	06	120

Table 3
Details of FE mesh of SESC-TP specimen.

Region	Element type	No. of elements	No. of nodes	No. of layers	No. of pallets
Tube like volume around the crack front	Solid-186	8640	37,189	06	120
Full model including tube like volume	Solid-186 and Solid-187	32,555	74,509	06	120

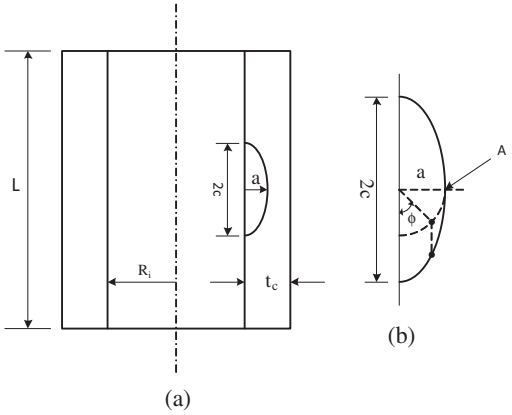

Fig. 12. (a) SESC-TP specimen, (b) crack tip position parameters in SESC-TP specimen.

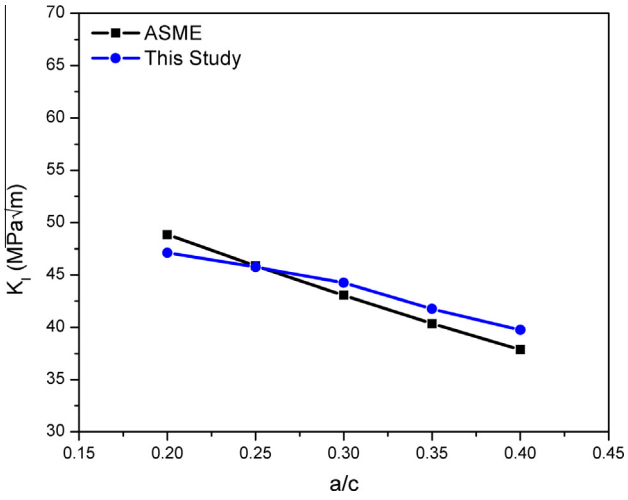

Fig. 14. Comparison of the developed fracture model with the ASME code.

For SESC-FP specimen, structural steel having $E = 200$ GPa and $v = 0.30$ was selected. The FE model of the SESC-FP specimen prepared for the fracture analysis is shown in Fig. 10. The details of the FE mesh of the SESC-FP specimen are given in Table 2.

The comparison with Newman and Raju analysis is done along the whole crack front of the semi-elliptical surface crack. The comparison (see Fig. 11) between the two methods shows a good agreement and the difference is within 5% along the whole crack front. It is also evident from Fig. 11 that the developed fracture model gave accurate results at the edge of the crack at $\phi = 0°$ or 180°. It is due to the development of small pallets around the whole crack front including crack edges as shown in Fig. 8(d).

4.2.2. Semi-elliptical surface cracks in thick pipe

The SIF solutions for semi-elliptical surface crack in internally pressurized thick pipe are available in Appendix D of Section VIII, Div. 3 of the ASME code [46]. According to Ref. [46], the SIF at the deepest point on the crack front may be calculated using the cubic polynomial stress relation given by Eq. (3):

$$K_I = \left[(A_o + A_p)G_o + A_1G_1 + A_2G_2 + A_3G_3\right]\sqrt{\frac{\pi a}{Q}} \tag{3}$$

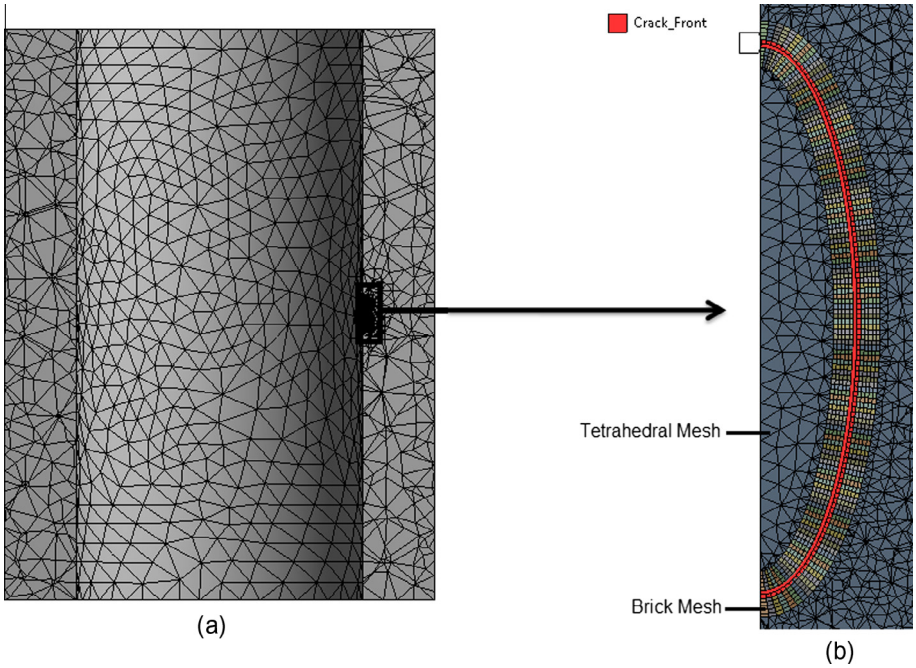

Fig. 13. FE mesh of SESC-TP specimen (b) Close-up view of crack region.

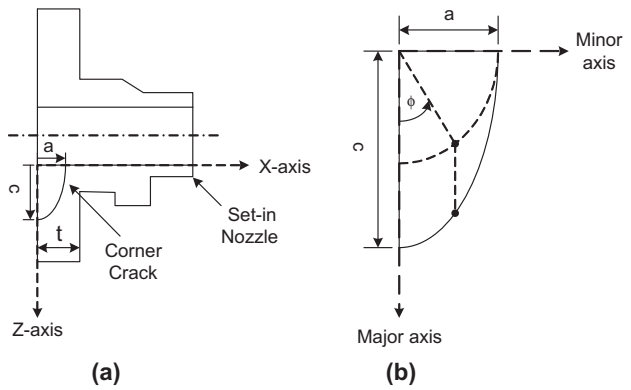

Fig. 15. (a) Orientation of the corner surface crack, (b) crack tip position parameters.

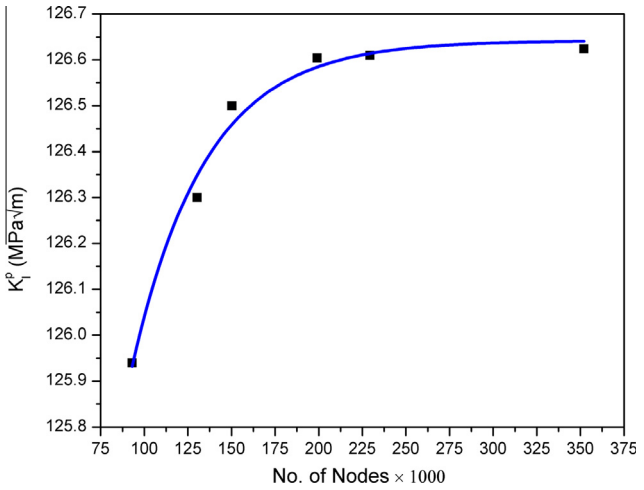

Fig. 17. Mesh independent study of the corner crack at the set-in nozzle-cylinder intersection when $a = 0.25t$, $a = 0.33c$.

where A_p = internal pressure if the pressure acts on the crack surface, A_i ($i = 0–3$) are the stress coefficients obtained from the through-the-thickness stress distribution, G_i ($i = 0–3$) are the geometrical correction factors as provided in ASME code [46].

The semi elliptical surface crack in thick pipe (SESC-TP) specimen given in Fig. 12(a) and (b), has the dimensions $L = 4000$ mm, $R_i = 1000$ mm, $t_c = 500$ mm, $a/t_c = 0.05$, $P_{int} = 50$ MPa. For SESC-TP specimen, structural steel having young modulus $E = 200$ GPa and Poisson's ratio $v = 0.30$ was selected. The FE model of the SESC-TP specimen prepared for the fracture analysis is shown in Fig. 13. The details of the FE mesh of SESC-TP specimen are given in Table 3.

The comparison with the method described in ASME code is done considering the $SIF_{I,max}$ value at the deepest point "A" of the surface crack as shown in Fig. 12(b). It is due to the fact that ASME code presents SIF solutions only at the deepest point of the surface crack in thick pipe. The comparison between the two approaches shows a good agreement, not exceeding a difference of 4% as shown in Fig. 14.

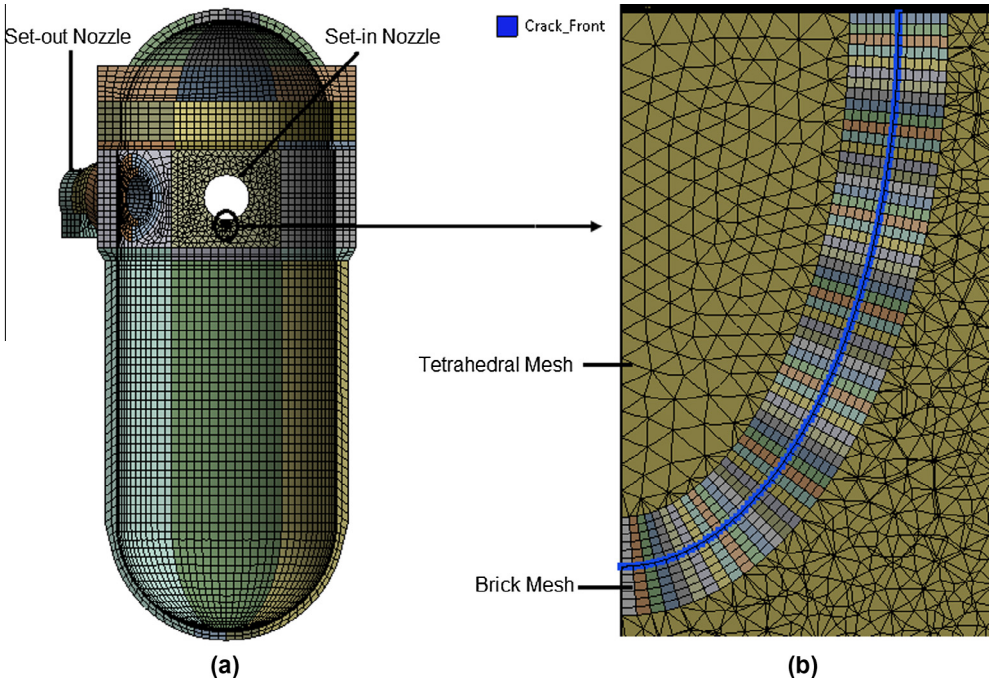

Fig. 16. (a) The FE model of the RPV having the corner crack at the set-in nozzle-cylinder intersection, (b) close-up view of crack region.

Table 4
Details of finite element mesh in RPV of PWR.

Region	Element type	No. of elements	No. of nodes	No. of layers	No. of pallets
Tube like volume around the crack front	Solid-186	4320	18,709	06	60
Half of the RPV including tube like volume	Solid-186 and Solid-187	134,207	229,403	06	60

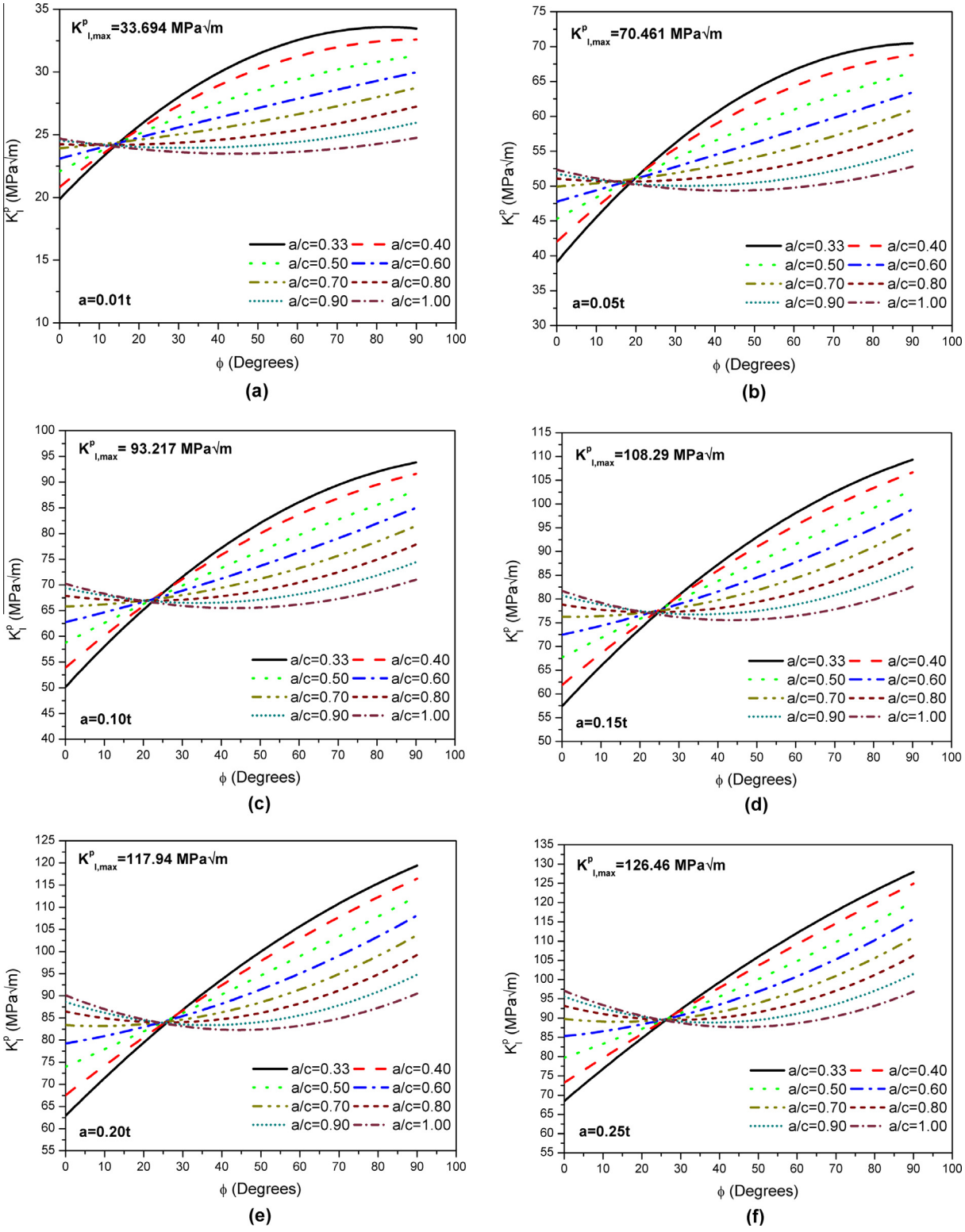

Fig. 18. SIFs along the whole corner crack fronts at the set-in nozzle-cylinder intersection under only the only pressure loadings.

The good agreement of the results with the standard studies gave confidence to use the developed fracture model for complex cases such as the elliptical corner surface cracks at HSCP of the RPV.

4.3. SIFs along the corner cracks under the only pressure loadings

For linear elastic fracture mechanics analysis, the forty-eight corner surface cracks of different dimensions were postulated at the set-in nozzle-cylinder intersection of the RPV. The orientation of the cracks is normal to the hoop stress in the RPV wall as shown in Fig. 15(a). The crack tip position parameters are shown in Fig. 15(b). The limits of the crack dimensions are $0.01 < a/t < 0.25$ and $0.33 < a/c < 1.0$, where "a" and "c" represent both semi-axis of the crack; and "$t = 309$ mm" is the thickness of the RPV wall at the set-in nozzle-cylinder intersection. The crack limits are designed to include the worst case crack having dimensions

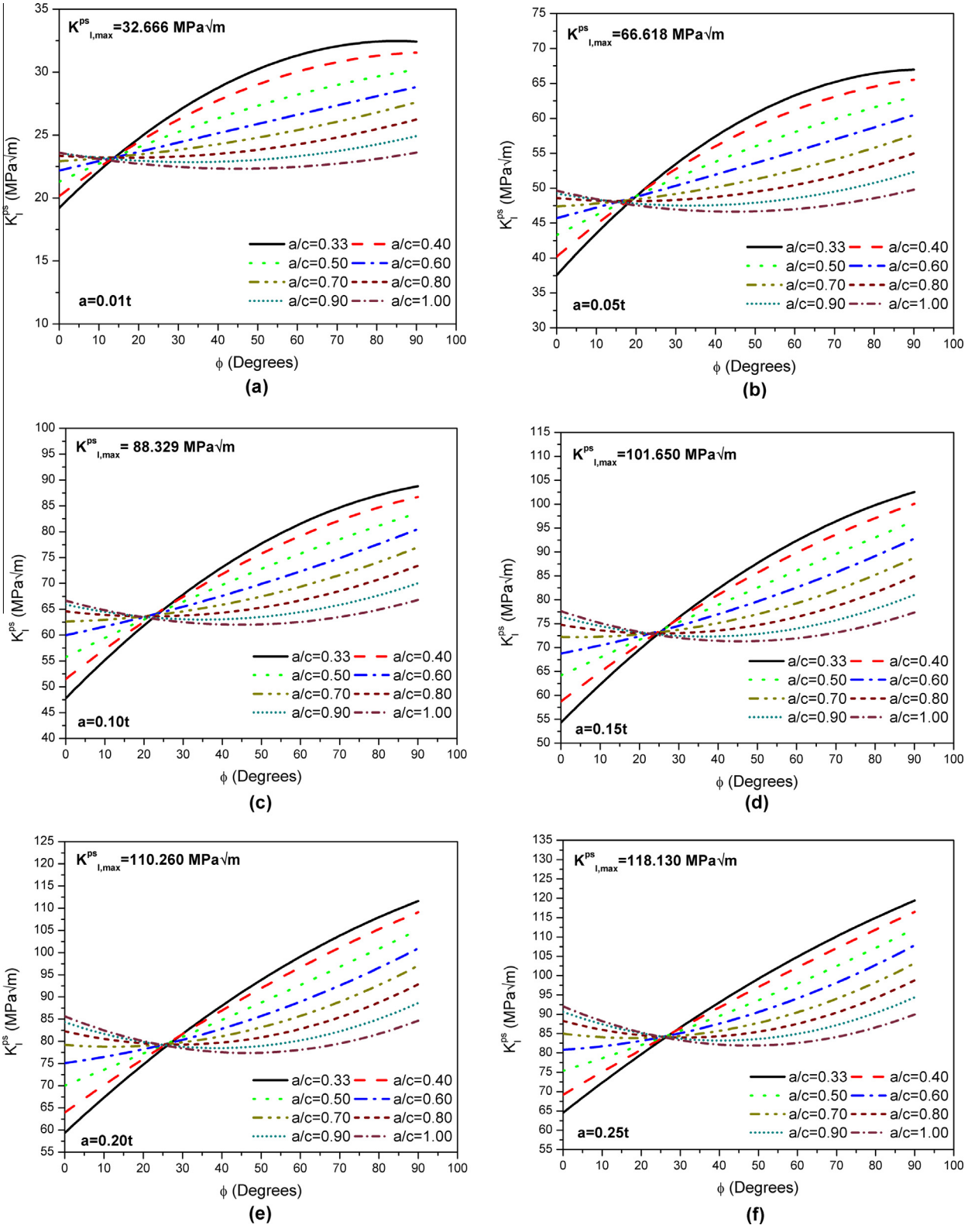

Fig. 19. SIFs along the whole corner crack fronts at the set-in nozzle-cylinder intersection under the combined loadings.

$a = 0.25t$ and $a = 0.33c$ allowed by the Appendix G ASME III, Div. 1 [27,40]. Using the technique presented in Section 4.1, the FE model of the cracked RPV is shown in Fig. 16. The details of the FE mesh of the RPV are provided in Table 4.

The basic mesh independent study was also performed for the worst case corner crack at the set-in nozzle-cylinder intersection. The exponentially growing trend has been achieved with the increase in number of nodes as shown in Fig. 17. Hence, the tech-

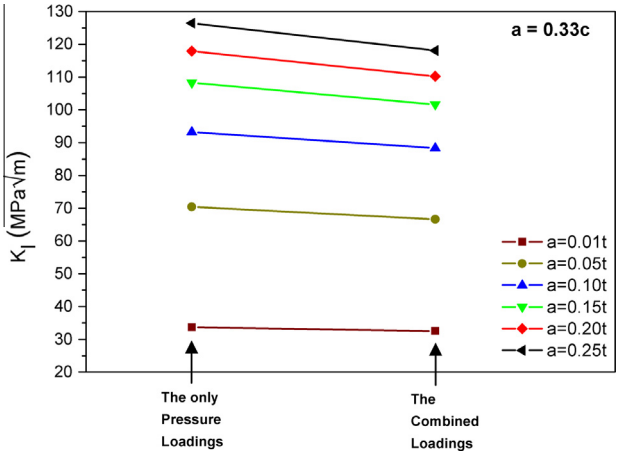

Fig. 20. Effect of the operational thermal stresses on SIFs of the corner crack at $a = 0.33c$.

nique used for the fracture modelling also yields good converging/mesh independent results.

The SIF solutions under the only pressure loadings (K_I^p) along the whole crack front for all the forty-eight cracks are presented in Fig. 18. It is clear from Fig. 18(a–f) that as the a/c ratio increases (for all values of a/t), K_I^p at $\phi = 0°$ also increases while K_I^p at $\phi = 90°$ decreases.

It is also evident from Fig. 18(a–f), that the SIFs of all the forty-eight cracks are lower than the fracture toughness value of the nuclear grade steel (SA-533 Gr.B, Cl.1) which is $K_{Ic} = 153\ \text{MPa}\sqrt{\text{m}}$ [30]. The worst allowed crack ($a = 0.25t$ and $a = 0.33c$) has $K_I^p = 126.46\ \text{MPa}\sqrt{\text{m}}$ (see Fig. 18(f)) which is much lower than the fracture toughness value of the selected material, so crack growth will not be feasible even taking into account the "worst scenario" considered by the ASME code [40]. That is why, the Westinghouse RPV made of SA-533 Gr.B, Cl.1 nuclear grade steel is a safe design even assuming the existence of the worst case crack at HSCP of the RPV allowed by the ASME code.

4.4. SIFs along the corner cracks under the combined loadings

The SIF solutions under the combined loadings (K_I^{ps}) along the whole crack front for all the forty-eight cracks are presented in Fig. 19. It is evident from Fig. 19(a–f) that the condition $K_I^{ps} < K_I^p$ is true for all the cracks. It is due to reason that in the RPV thermal stresses in the hoop direction (see Fig. 6(b)) are compressive at the inner surface of the cylinder; i.e., the material in this region "wants to grow" but is restricted by the adjacent material at the lower temperature. Hence, the compressive hoop stresses at the set-in nozzle-cylinder intersection of the RPV minimize the mechanical tensile hoop stresses (crack opening stresses) due to internal pressure. The reduction of crack opening stresses finally leads lesser SIFs.

The six corner cracks having $a = 0.33c$ for all six "a/t" ratios are taken to present the effect of the operational thermal stresses. The decreasing slope of all the lines in Fig. 20, predicts that the operational thermal stresses reduce the SIF of the corner cracks at the set-in nozzle-cylinder intersection of the RPV. Hence, it can be concluded that the operational thermal stresses caused by the provision of annular chamber of air between the RPV and the RVI (see Fig. 3(b)) for ERVC actually reduce the SIFs due to the only pressure loadings (K_I^p) and they do not endanger the safety of the RPV. Therefore, the application of the annular chamber for the ERVC can be fully successful and safe from fracture mechanics point of view.

5. Conclusions

The SIF solutions of corner elliptical surface cracks postulated at the HSCP of the RPV of the PWR have been obtained numerically. The SIF solutions under the only pressure and the combined (pressure plus thermal) loadings are presented in a graphical format, suitable for the fracture mechanics design of RPV. The numerical technique has been verified by comparing the results to the available numerical results of Newman and Raju and ASME code. The main conclusions drawn from the study can be summarized as follows:

- The Westinghouse RPV made of SA-533 Gr.B, Cl.1 nuclear grade steel is a safe design even assuming the existence of the worst case crack at the HSCP of the RPV allowed by the ASME code.
- The application of the annular chamber between the RPV and the RVI for external reactor vessel cooling is fully successful and safe from the fracture mechanics point of view. It is due to reason that the operational thermal stresses caused by the provision of the annular chamber of the air for the ERVC actually reduce SIF of the corner cracks due to the only pressure loadings (K_I^p) and they do not endanger the safety of the RPV.

Acknowledgements

The financial support of Pakistan Institute of Engineering and Applied Sciences for this study under IT & Telecom Endowment Fund is gratefully acknowledged.

References

[1] K. Ramesh, D.P.S. Chanchan, A.K. Malik, Free vibration of an annular plate with periodic radial cracks, J. Sound Vib. 206 (2) (1997) 266–274.
[2] K. Ramesh, S. Gupta, A.A. Kelkar, Evaluation of stress field parameters in fracture mechanics by photoelasticity-revisited, Eng. Fract. Mech. 56 (1) (1997) 25–45.
[3] K. Ramesh, S. Shukla, P.M. Dixit, N. Karuppaiah, Numerical evaluation of SIF for radial cracks in thick annular ring using cyclic symmetry, Eng. Fract. Mech. 56 (2) (1997) 141–153.
[4] M. Uslu, O. Demir, A.O. Ayhan, Surface cracks in finite thickness plates under thermal and displacement-controlled loads – part 1: stress intensity factors, Eng. Fract. Mech. 115 (2014) 284–295.
[5] G.R. Irwin, Crack extension force for a part - through crack in a plate, J. Appl. Mech. 29 (1962) 651–654.
[6] F.W. Smith, A.F. Emery, A.S. Kobayashi, Stress intensity factors for semicircular cracks Part 2 – semi-infinite solid, J. Appl. Mech. 34 (1967) 947–952.
[7] R.W. Thresher, F.W. Smith, Stress intensity factors for a surface crack in a finite solid, J. Appl. Mech. 39 (1972) 95–200.
[8] C.Y. Liao, S.N. Atluri, Stress intensity factor variation along a semicircular surface flaw in a finite-thickness plate, Eng. Fract. Mech. 34 (1989) 957–976.
[9] T.A. Cruse, Application of the boundary-integral equation method to three dimensional stress analysis, Comput. Struct. 3 (1973) 509–527.
[10] C. Guozhong, Z. Kangda, Stress intensity factor for semi-elliptical surface cracks in plates and cylindrical pressure vessels using the hybrid boundary element method, Eng. Fract. Mech. 52 (1995) 1035–1054.
[11] C. Guozhong, Z. Kangda, Stress intensity factors for internal semi elliptical surface cracks in pressurized thick walled cylinders using the hybrid boundary element methods, Eng. Fract. Mech. 52 (1995) 1055–1064.
[12] W.S. Blackburn, T.K. Hellen, Calculation of stress intensity factors in three dimensions by finite element methods, Int. J. Numer. Meth. Eng. 11 (1972) 211–229.
[13] H.G. Delorenzi, Energy release rate calculations by the finite element method, Eng. Fract. Mech. 21 (1985) 129–143.
[14] T. Fett, Estimation of stress intensity factors for semi-elliptical surface cracks, Eng. Fract. Mech. 66 (2000) 349–356.
[15] J.R. Rice, N. Levy, The part-through surface crack in an elastic plate, J. Appl. Mech. 39 (1972) 185–194.
[16] F. Erdogan, B. Aksel, Line spring model and its applications to part-through crack problems in plates and shells, NASA Contractor Report 178141 LEHIGH University Bethlehemj Pennsylvania, June 1986.
[17] R. Sethuraman, I.T. Ilango, Analysis of interacting semi-elliptical surface cracks in finite thickness plates under remote bending load, Int. J. Press. Vess. Pip. 82 (2005) 528–545.
[18] B.E.K. Hachi, S. Rechak, Y. Belkacemi, G. Maurice, Modeling of elliptical cracks in an infinite body and in a pressurized cylinder by a hybrid weight function approach, Int. J. Press. Vess. Pip. 82 (2005) 917–924.

[19] A.O. Ayhan, Mixed mode stress intensity factors for deflected and inclined corner cracks in finite-thickness plates, Int. J. Fatigue 29 (2007) 305–317.
[20] A.O. Ayhan, Simulation of three-dimensional fatigue crack propagation using enriched finite elements, Comput. Struct. 89 (2011) 801–812.
[21] E. Nart, A.O. Ayhan, Crack insertion, meshing and fracture analysis of structures using tetrahedral finite elements, Eur. J. Mech. A/Solids 30 (2011) 293–306.
[22] M. Uslu, O. Demir, A.O. Ayhan, Surface cracks in finite thickness plates under thermal and displacement controlled loads – Part 2: crack propagation, Eng. Fract. Mech. 115 (2014) 255–269.
[23] M. Kamaya, Stress intensity factors of surface crack with undulated front, JSME Int. J. – Ser. A 49 (2006) 529–535.
[24] J.C. Newman Jr., I.S Raju, Stress-intensity factor equations for cracks in three-dimensional finite bodies subjected to tension and bending loads, in: AtluriS (Ed.), Comput Method Mech Fract, vol. 2, Elsevier Science Publishers, Amsterdam, 1986, pp. 311–334.
[25] R. Sandstrom, P. Langenberg, H. Sieurin, New brittle fracture model for the European pressure vessel standard, Int. J. Press. Vess. Pip. 81 (2004) 837–845.
[26] A.T. Diamantoudis, G.N. Labeas, Stress intensity factors of semi-elliptical surface cracks in pressure vessels by global–local finite element methodology, Eng. Fract. Mech. 72 (2005) 1299–1312.
[27] M.A. Guerrero, C. Betegon, J. Belzunce, Fracture analysis of a pressure vessel made of high strength steel (HSS), Eng. Fail. Anal. 15 (2008) 208–219.
[28] J. Chen, H. Pan, Stress intensity factor of semi-elliptical surface crack in a cylinder with hoop wrapped composite layer, Int. J. Press. Vess. Pip. 30 (2013) 1–5.
[29] J. Predan, V. Mocilnik, N. Gubeljak, Stress intensity factors for circumferential semi-elliptical surface cracks in a hollow cylinder subjected to pure torsion, Eng. Fract. Mech. 105 (2013) 152–168.
[30] Y. Bangash, PWR steel pressure vessel design and practice, Prog. Nucl. Energy 16 (1) (1985) 1–40.
[31] M.J. Jhung, Y.W. Park, C. Jang, Pressurized thermal shock analyses of a reactor pressure vessel using critical crack depth diagrams, Int. J. Press. Vess. Pip. 76 (1999) 813–823.
[32] Y. He, T. Isozaki, Fracture mechanics analysis and evaluation for the RPV of the Chinese Qinshan 300 MW NPP under PTS, Nucl. Eng. Des. 201 (2000) 121–137.
[33] O.Ö. Gülol, Ü. Çolak, Comparison of pressure vessel integrity analyses and approaches for VVER 1000 and PWR vessels for PTS conditions, Nucl. Eng. Des. 226 (2003) 231–241.
[34] M. Chen, F. Lu, R. Wang, A. Ren, Structural integrity assessment of the reactor pressure vessel under the pressurized thermal shock loading, Nucl. Eng. Des. 272 (2014) 84–91.
[35] ASME Boiler and Pressure Vessel Code, Section III, Division 1: Rules for construction of nuclear facility components, New York, 2010.
[36] ESS, Assessment and management of ageing of major nuclear power plant components important to safety: PWR pressure vessels, International Atomic Energy Agency, IAEA-TECDOC-1120, 1999.
[37] B.R. Sehgal, Stabilization and termination of severe accidents in LWRs, Nucl. Eng. Des. 236 (2006) 1941–1952.
[38] J.S. Kim, T.E. Jin, Structural integrity assessment of the reactor pressure vessel under the external reactor vessel cooling condition, Nucl. Eng. Des. 191 (1999) 117–133.
[39] J.W. Park, Analytical evaluation of two-phase natural circulation flow characteristics under external reactor vessel cooling, Ann. Nucl. Energy 36 (2009) 1668–1675.
[40] ASME Boiler and Pressure Vessel Code, Section III, Division 1, Appendix G: Fracture toughness criteria for protection against failure, New York, 2010.
[41] ASME Boiler and Pressure Vessel Code, Section II, Part D: Properties (Metric) Materials, New York, 2010.
[42] H.H. Lee, Finite element simulations with ANSYS Workbench 14, Stephen Schroff, 2012.
[43] C.F. Shih, B. Moran, T. Nakamura, Energy release rate along a three-dimensional crack front in a thermally stressed body, Int. J. Fract. 30 (1986) 79–102.
[44] K. Ramesh, E-Book on Engineering Fracture Mechanics, in, IIT Madras, 2007.
[45] J.C. Newman, I.S. Raju, An empirical stress intensity factor equation for the surface crack, Eng. Fract. Mech. 15 (1981) 185–192.
[46] ASME Boiler and Pressure Vessel Code, Section VIII, Division 3, Non Mandatory Appendix D: Fracture mechanics calculations, New York, 2010.